

# Growth and Laser Modulation Properties of $\text{KTa}_{0.63}\text{Nb}_{0.37}\text{O}_3$ Single Crystals

BING LIU<sup>a,b</sup>, HUADI ZHANG<sup>a,b</sup>, YUANYUAN ZHANG<sup>a,b</sup>, XIANSUN LV<sup>a,b</sup>, YUGUO YANG<sup>a,b,\*</sup>,  
LEI WEI<sup>a,b</sup>, XUPING WANG<sup>a,b</sup>, HUAJIAN YU<sup>a,b</sup>, CONG ZHANG<sup>a,b</sup> AND JING LI<sup>a,c</sup>

<sup>a</sup>Advanced Materials Institute, Qilu University of Technology (Shandong Academy of Sciences), Jinan 250014, China

<sup>b</sup>Qilu University of Technology (Shandong Academy of Sciences), Advanced Materials Institute, Key Laboratory for Light Conversion Materials and Technology of Shandong Academy of Sciences, Jinan 250014, China

<sup>c</sup>Qilu University of Technology (Shandong Academy of Sciences), Advanced Materials Institute, Shandong Provincial Key Laboratory for High Strength Lightweight Metallic Materials, Jinan 250014, China

(Received April 19, 2017; in final form August 20, 2018)

$\text{KTa}_{0.63}\text{Nb}_{0.37}\text{O}_3$  (KTN) single crystals were grown by a top seeded solution growth method. We found that the composition variation of crystal is smaller if the weight of melting raw materials is larger. The phase, dielectric property, and transmittance of the grown KTN single crystals were investigated. The dependence of dielectric constant on temperature indicated that crystal chips cutting from the shoulder, body, and bottom both have the same  $T_c$  value of 17 °C, which suggests the homogeneity of the grown crystals. The laser modulation using a KTN chip indicates potential applications in deflectors due to the advantage of high angular accuracy.

DOI: [10.12693/APhysPolA.135.396](https://doi.org/10.12693/APhysPolA.135.396)

PACS/topics: KTN single crystal, TSSG, homogeneity, laser modulation

## 1. Introduction

$\text{KTa}_{1-x}\text{Nb}_x\text{O}_3$  (KTN) is a ferroelectric material and its dielectric constant and quadratic electro-optic (EO) constant (the Kerr constant) are maximum around the paraelectric to ferroelectric phase transition temperature ( $T_c$ ) [1]. KTN crystals show quadratic EO coefficients of  $10^{-14} \text{ m}^2 \text{ V}^2$  in magnitude, response times of nanoseconds, broad transmittance of 400–4000 nm, and a high diffraction efficiency of 80% [2]. These excellent properties of KTN crystals lead to potential applications in some fields. In 2007, Nakamura reported the achievement of large angle and low-voltage electro-optic beam scanning using KTN crystal [3]. In 2008, Tang et al. also reported a high-speed electro-optic beam scanner based on KTN crystal [4]. In 2012, Okabe et al. presented a new light source for swept-source optical coherence tomography (SS-OCT) using a KTN electro-optic deflector [5]. In 2015, using lithium-enriched potassium-tantalate-niobate (KTN:Li) crystals as propagation medium, DelRe et al. created subdiffraction-limit-sized optical beams propagating over several mm and the beams shrink rather than expand in propagation [6], which overcomes the fundamental wave phenomenon of diffraction [7]. In these studies focusing on KTN, the successful growth of KTN single crystal with high quality makes it possible to perform various optical measurements.

The solid solution of KTN crystallizes only in perovskite structure for all compositions [8]. Due to the

similar valence state and ionic radii of Ta and Nb, the primary growth difficulties are the compositional fluctuation and striation. Researchers have attempted some techniques to overcome these growth difficulties, such as step-cooling technique [8], constant temperature method [9], temperature gradient transport growth technique [10], the Czochralski method [1] and top-seeded solution growth (TSSG) method [11]. In this work, we grew KTN single crystals by TSSG method. The TSSG method combines the growth methods of Czochralski and solution growth, which is good to grow crystals requiring decomposition before melting or having too high melting point to grow from original composition [12]. The relating properties of the grown single crystals have been investigated carefully.

## 2. Theory analysis

Figure 1 gives the phase diagram of KTN, which shows  $\text{KNbO}_3$  and  $\text{KTaO}_3$  system does not have a congruent melting point. As a result, the ratio of Ta/Nb changes with the changing growth temperature, which means the impossibility of growth for KTN crystal with a constant Ta/Nb ratio. Herein, we match the liquid-phase line and solid-phase line and obtain the equations between equilibrium temperature and solid-phase composition. For the solid-phase line, we obtain the equation

$$T = a_1x^3 + b_1x^2 + c_1x + d_1, \quad (1)$$

where  $a_1 = -102.4$ ,  $b_1 = 383$ ,  $c_1 = -596.3$ ,  $d_1 = 1352$  and  $x$  represents the Nb concentration in KTN. For the liquid-phase line, we obtain the equation

$$T = a_2X^3 + b_2X + c_2X + d_2, \quad (2)$$

where  $a_2 = -132.2$ ,  $b_2 = 11.5$ ,  $c_2 = -198.5$ ,  $d_2 = 1352$  and  $X$  represents the Nb concentration in liquid solution.

\*corresponding author; e-mail: [yangyuguo@sdas.org](mailto:yangyuguo@sdas.org)

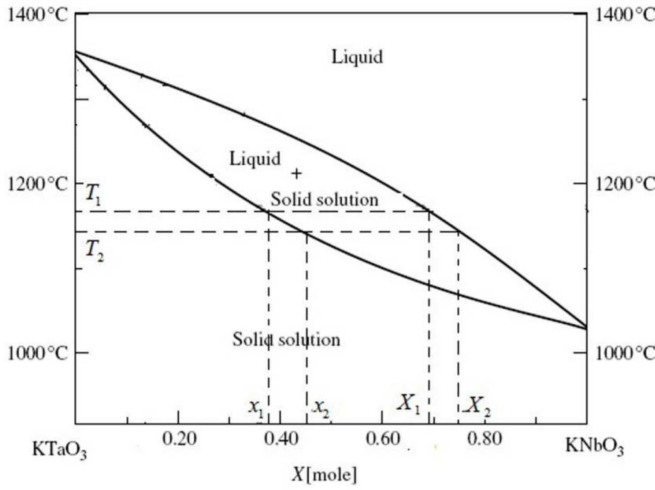


Fig. 1. Phase diagram of KTN.

Thus, the change of crystal constituent induced by the decrease of temperature can be expressed as

$$\Delta x = (dx/dx)\Delta T. \quad (3)$$

From these, we can conclude that the composition variation of a grown KTN crystal in a certain temperature region depends on the primary composition of KTN crystal.

Generally speaking, the composition variation of a grown KTN crystal leads to the formation of growth striation, which is one of the major defects affecting the properties of KTN [13]. To overcome it, one of the methods is to grow KTN crystal, in as many melting raw material as possible. Herein, we choose an Nb concentration of 0.37 as an example to elaborate it. Based on Eqs. (1)–(3), we can calculate a result of  $dx/dT = 1.82 \times 10^{-3} \text{ }^\circ\text{C}$ . As shown in Fig. 1, the initial composition should be  $X_1 \approx 0.68$  if the crystal growth is carried out at an equilibrium temperature. The value of equilibrium temperature should be at  $1180^\circ\text{C}$ , if the distribution of raw materials in melt is homogeneous. Based on the lever principle, we can obtain the equation in a temperature region of  $T_1 - T_2$ :

$$m(X_1 - x_1) = (M - m)(X_2 - X_1), \quad (4)$$

where  $m$  is the weight of the obtained KTN crystal,  $M$  is the weight of raw materials,  $x_1$  is the Nb concentration in the KTN crystals based on primitively raw material,  $X_1$  is the Nb concentration in the primitively raw materials,  $x_2$  is the Nb concentration in the KTN crystals based on the residual raw materials and  $X_2$  is the Nb concentration in the residual raw materials. When the temperature region is small, we can obtain a result of  $X_1 - x_2 \approx X_1 - x_1 \approx 0.31$  because  $M \gg m$ . Thus, Eq. (4) can be simplified as

$$m = M(X_2 - x_1)/0.31. \quad (5)$$

From Eq. (2), we can calculate the result of  $\Delta T/\Delta x = -358.9$  if  $X_1 \approx 0.68$ . We subsequently obtain another equation through Eq. (5):

$$m = 8.988 \times 10^{-3} M(T_1 - T_2). \quad (6)$$

It is known that the density of  $\text{KTa}_{0.63}\text{Nb}_{0.37}\text{O}_3$  is  $6.25 \text{ g/cm}^3$ . Thus, Eq. (6) can be changed to be

$$V = 1.438 \times 10^{-3} M(T_1 - T_2). \quad (7)$$

From Eqs. (3) and (7), we can know that the composition variation is smaller if the weight of melting raw materials is larger.

### 3. Crystal growth and characterization

$\text{KTa}_{0.63}\text{Nb}_{0.37}\text{O}_3$  single crystals were grown by a TSSG method.  $\text{K}_2\text{CO}_3$ ,  $\text{Ta}_2\text{O}_5$ , and  $\text{Nb}_2\text{O}_5$  with purities of 99.99% were used as raw materials in the crystal growth. In a typical growth process, raw materials of  $\text{Ta}_2\text{O}_5$  and  $\text{Nb}_2\text{O}_5$  were well according with the stoichiometric proportion but the weight of  $\text{K}_2\text{CO}_3$  was in excess of 10%. The crystals were grown in a TDL-H50AC crystal-pulling apparatus. A rectangular KTN single crystal bar with dimensions of  $3 \text{ mm} \times 3 \text{ mm} \times 30 \text{ mm}$  was used as the seed. The pulling rate was kept at  $0.5 \text{ mm/h}$ , when the crystal diameter reached a certain value. The crystal was rotated at a rate of  $5 \text{ rpm}$  during growth. After the growth was completed, the crystal was cooled to room temperature at a speed of  $30^\circ\text{C/h}$ . High quality single crystals of  $20\text{--}30 \text{ mm}$  in length were grown in a week's running time.

The as-grown KTN single was oriented firstly. The rectangular KTN chips were cut from the shoulder, body, and bottom of an as-grown KTN crystal and all surfaces of the chip are normal to a crystal axis. Then, the chips were mirror polished. The final sizes of the polished chips were  $2.8 \text{ mm} \times 1.2 \text{ mm} \times 7.5 \text{ mm}$  with the largest faces perpendicular to the  $[100]$  direction. X-ray diffraction (XRD) was performed on a Rigaku D/Max-3C X-ray diffractometer with high-intensity  $\text{Cu } K_\alpha$  radiation. The compositions were measured by electron microprobe analysis. The transmittance was measured using a Cary 50 UV-visible spectrophotometer. The dielectric properties were measured as a function of temperature using a TH2827C LCR meter. All measurements, except the dielectric properties, were carried out at room temperature.

### 4. Results and discussion

Figure 2 gives an image of a grown  $\text{KTa}_{0.63}\text{Nb}_{0.37}\text{O}_3$  single crystal. It can be seen that the crystal is colorless and transparent, and has a prismatic shape. Some defects, such as bubbles, nebulous inclusions, and hollows will appear in the grown crystal if the growth conditions are not suitable to equably grow. We found that the sintering temperature, sintering time, pulling rate, and rotation rate have obvious influence on the properties of crystals [1]. The results of our work suggest that crystals having excellent properties are grown by controlling growth parameters. The compositions of the crystal chips cutting from shoulder, body, and bottom were estimated by electron microprobe analysis, showing that the

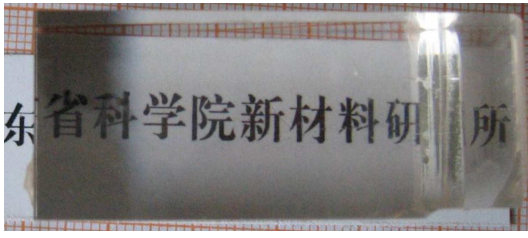


Fig. 2. Image of a grown  $\text{KTa}_{0.63}\text{Nb}_{0.37}\text{O}_3$  single crystal.

Nb composition difference is less than  $2.0 \times 10^{-4}/\text{mm}$  along the growth direction. Figure 3 shows the XRD patterns of the grown  $\text{KTa}_{0.63}\text{Nb}_{0.37}\text{O}_3$  single crystal, which is well according with the data of JCPDs card no. 70–2011. There are no diffraction peaks corresponding to other phase, indicating that the pure perovskite phase is obtained. The sharp diffraction peaks demonstrate the high crystalline of the  $\text{KTa}_{0.63}\text{Nb}_{0.37}\text{O}_3$  crystal.

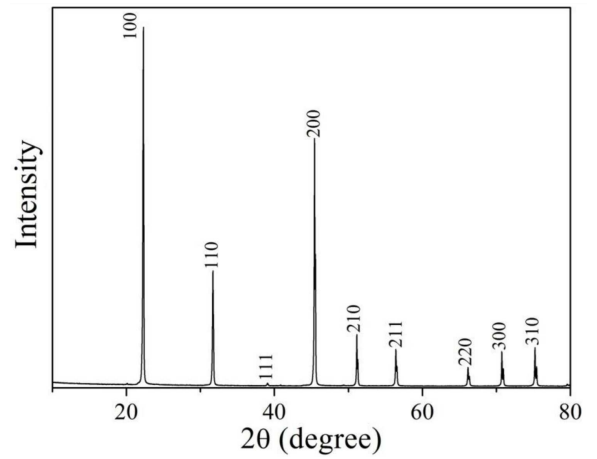


Fig. 3. XRD patterns of a grown  $\text{KTa}_{0.63}\text{Nb}_{0.37}\text{O}_3$  single crystal.

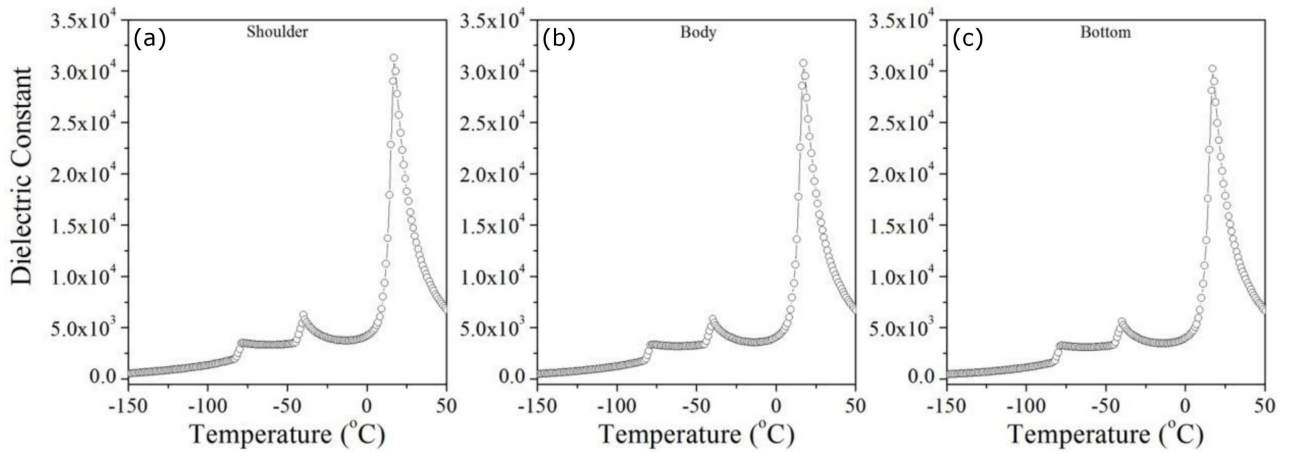


Fig. 4. Dielectric curves of three crystal chips cutting from shoulder, body and bottom of a grown  $\text{KTa}_{0.63}\text{Nb}_{0.37}\text{O}_3$  crystal.

The Ta/Nb composition ratio also can be estimated by the phase transition temperature. In earlier years, Nakamura et al. reported the relations between the crystal phase, temperature, and Ta/Nb composition ratio, showing that the  $T_c$  of  $\text{KTa}_{0.63}\text{Nb}_{0.37}\text{O}_3$  is about  $17^\circ\text{C}$  [14, 15]. Figure 4 shows the dependence of dielectric constant on temperature for three crystal samples cutting from shoulder, body, and bottom at the frequency of 1000 Hz. Both dielectric curves of three crystal samples consist of three dielectric peaks in the temperature region of  $(-150)\text{--}50^\circ\text{C}$ , which correspond to the four phase transitions. The dielectric peak at about  $-78^\circ\text{C}$  is induced by the phase transition from rhombohedral phase to orthorhombic phase. The dielectric peak at about  $-40^\circ\text{C}$  is induced by the phase transition from orthorhombic phase to tetragonal phase. The dielectric peak at about  $17^\circ\text{C}$  is induced by the phase transition from tetragonal phase to cubic phase. At about  $17^\circ\text{C}$ , the dielectric constant reaches a maximum and this dielectric peak origi-

nates from the ferroelectric–paraelectric phase transition. It can be seen from Fig. 4 that both crystal chips have a high dielectric constant value of more than  $3.0 \times 10^4$  and a  $T_c$  value about  $17^\circ\text{C}$ . It is known that KTN is a solid state solution of  $\text{KTaO}_3$  and  $\text{KNbO}_3$ . The  $T_c$  value of KTN depends on the Ta/Nb ratio [14]. The same  $T_c$  values suggest the same Ta/Nb ratio and thus indicate the homogeneity of the grown crystals. Generally speaking, the dielectric constants of lead-free perovskite single crystals are usually much lower than those of lead-based single crystals [15]. However, the dielectric constant value of the grown  $\text{KTa}_{0.63}\text{Nb}_{0.37}\text{O}_3$  crystal is higher than that of  $\text{Pb}(\text{Mg}_{1/3}\text{Nb}_{2/3})\text{O}_3\text{--PbTiO}_3$  ferroelectric [16], suggesting the potential applications of KTN in various fields.

KTN is one of the materials having excellent electro-optic effect. The electro-optic effect refers to a phenomenon that the refractive index of a material can be regulated by an external electric field and the Pockels and

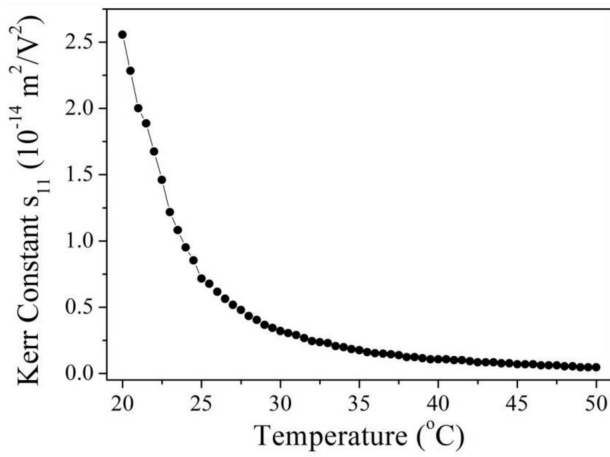


Fig. 5. Dependence of  $s_{11}$  on temperature for crystal chip cutting from bottom of a grown  $KTa_{0.63}Nb_{0.37}O_3$  crystal.

Kerr effects are the two main electro-optic effects [17]. The Kerr effect of a material can be reflected by the Kerr constant  $s_{ij}$ . The values of  $s_{ij}$  at different temperatures have close relation with its dielectric constants, which can be written as a formula

$$s_{ij} = g_{ij}\epsilon_0^2(\epsilon_r - 1)^2 \approx g_{ij}\epsilon_0^2\epsilon_r^2 = g_{ij}\epsilon^2 \quad (\epsilon_r \gg 1),$$

where  $\epsilon_0$  is the vacuum permittivity and  $g_{ij}$  is the  $g$  coefficient [18]. The  $g$  coefficient depends on the wavelength but does not depend on  $\epsilon_r$ , the frequency of the external electric field, and temperature. The  $g$  coefficients of KTN are  $g_{11} = 0.136 \text{ m}^4/\text{C}^2$  and  $g_{12} = -0.038 \text{ m}^4/\text{C}^2$  [19]. Figure 5 gives the dependence of  $s_{11}$  on temperature performing on a low frequency sinusoidal voltage of 10 Hz for crystal chip cutting from bottom. The maximal value of  $s_{11}$  reaches to be  $2.56 \times 10^{-14} \text{ m}^2/\text{V}^2$ . The high value of  $s_{11}$  is induced by the homogeneity of the grown  $KTa_{0.63}Nb_{0.37}O_3$  crystal.

The image (Fig. 1) of a grown  $KTa_{0.63}Nb_{0.37}O_3$  crystal shows that it is transparent. Figure 6 gives the transmittance spectra of crystal chips cutting from shoulder, body and bottom of a grown  $KTa_{0.63}Nb_{0.37}O_3$  crystal, which shows that the three crystal chips have high transmittance in visible light region and it is completely opaque at about 380 nm. The complete opaqueness suggests the band gap energy of a material. The photon energy of the near-infrared light is too low to activate electrons to move through the band gap, indicating that the energy of photon is not absorbed by the crystal. Since the band gaps of  $KNbO_3$  and  $KTaO_3$  are 3.14 eV and 3.42 eV, and the basic energy levels of KTN are determined by the  $NbO_6$  and  $TaO_6$  groups [20, 21], the same band gaps of three crystal chips also indicate the homogeneity of the grown  $KTa_{0.63}Nb_{0.37}O_3$  crystal.

One of attractive applications of the electro-optic effect is laser modulation. Some laser beam characteristics, such as intensity of laser beam, direction of propa-

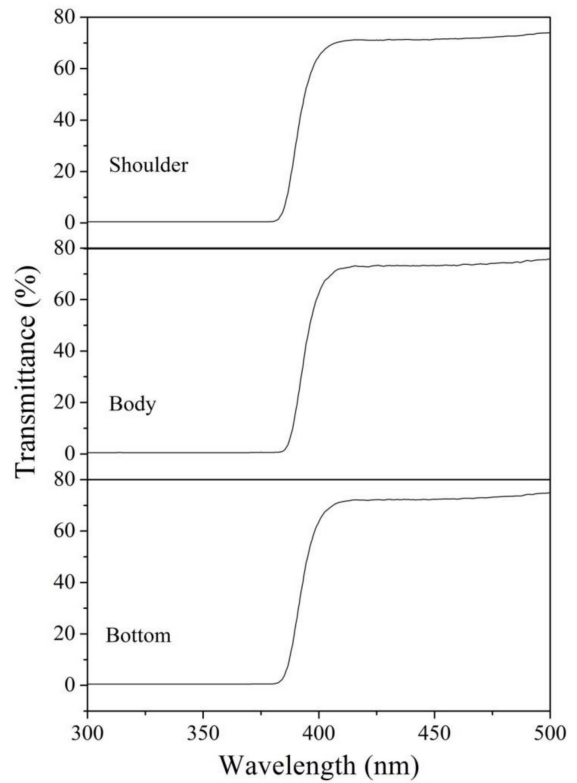


Fig. 6. Transmittance spectra of crystal chips cutting from shoulder, body and bottom of a grown  $KTa_{0.63}Nb_{0.37}O_3$  crystal.

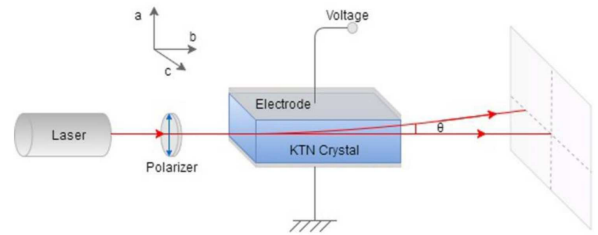


Fig. 7. Schematic of the experimental setup used in the measurements of laser modulation.

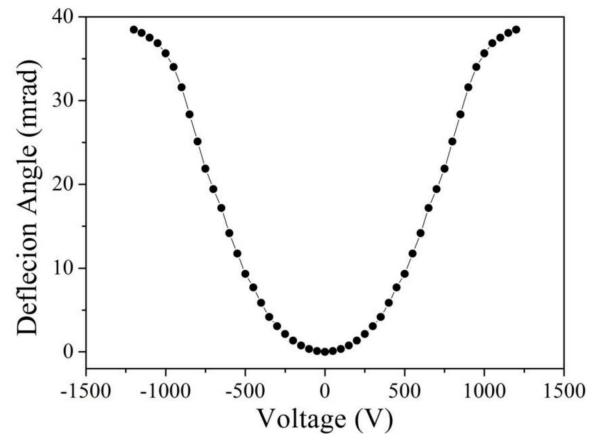


Fig. 8. Dependence of deflection angle on the external electric field.

gation, can be modulated through a crystal material having excellent electro-optic effect. We also investigated the laser modulation of KTN using a  $\text{KTa}_{0.63}\text{Nb}_{0.37}\text{O}_3$  crystal chip cutting from the bottom by the experimental setup shown in Fig. 7. The maximum values of the external electric field are  $\pm 1200$  V. The experiments were carried at  $20^\circ\text{C}$ , which is about  $3^\circ\text{C}$  higher than the  $T_c$  of  $\text{KTa}_{0.63}\text{Nb}_{0.37}\text{O}_3$  crystal. At this temperature,  $\text{KTa}_{0.63}\text{Nb}_{0.37}\text{O}_3$  is in the cubic phase and the lowest electro-optic effect is the quadratic Kerr effect. Figure 8 shows the dependence of deflection angle on the external electric field. The deflection angle increases with the increasing external electric field and there is no change of deflection direction if we reverse the external electric field direction. Hence, we can control the beam deflection angle by controlling the external electric field. The maximum deflection angle of electro-optical deflectors based on KTN single crystal is smaller than those of mirror based deflectors. However, the angular accuracy of electro-optical deflectors based on KTN single crystal is higher than those of mirror based deflectors and the random-access response time is smaller [22]. This indicates the wide potentials of applications of KTN in deflectors.

## 5. Conclusion

We have grown highly homogeneous  $\text{KTa}_{0.63}\text{Nb}_{0.37}\text{O}_3$  single crystals by a TSSG method, which is demonstrated by the dielectric property of three crystal samples. The dependence of dielectric constant on temperature indicates that crystal samples cutting from the shoulder, body, and bottom both have a  $T_c$  value of  $17^\circ\text{C}$ , which suggests the homogeneity of the grown crystals. The maximal value of  $s_{11}$  reaches to be  $2.56 \times 10^{-14} \text{ m}^2/\text{V}^2$ , meaning an excellent Kerr effect of the  $\text{KTa}_{0.63}\text{Nb}_{0.37}\text{O}_3$  single crystal. Laser modulation is obtained through a  $\text{KTa}_{0.63}\text{Nb}_{0.37}\text{O}_3$  crystal chip by controlling the external electric field. The performance of deflector based on KTN crystal leads to its positive application in fields of imaging, sensing, and telecommunication.

## Acknowledgments

This work was supported by the General Program of National Natural Science Foundation of China (51672164 and 51772172); Major scientific and technological innovation project in Shandong (2018CXGC0412); Natural Science Foundation of Shandong Province (ZR2016EMM12, ZR2017MEM016, ZR2017BEM043, ZR2018BEM023 and ZR2018PEM006); Youth Foundation of Shandong Academy of Sciences (2018QN0033).

## References

- [1] X. Wang, J. Wang, Y. Yu, H. Zhang, R.I. Boughton, *J. Cryst. Growth* **293**, 398 (2006).
- [2] P. Tan, H. Tian, C. Mao, C. Hu, X. Meng, L. Li, G. Shi, Z. Zhou, *Appl. Phys. Lett.* **111**, 012903 (2017).
- [3] K. Nakamura, *NTT Techn. Rev.* **5**, 1 (2007).
- [4] Y. Tang, J. Wang, X. Wang, B. Duan, S. Tang, *Proc. SPIE* **7135**, 713538 (2008).
- [5] Y. Okabe, Y. Sasaki, M. Ueno, T. Sakamoto, S. Toyoda, S. Yagi, K. Naganuma, K. Fujiura, Y. Sakai, J. Kobayashi, K. Omiya, M. Ohmi, M. Haruna, *Electron. Lett.* **48**, 201 (2012).
- [6] E. DelRe, F. Di Mei, J. Parravicini, G. Parravicini, A.J. Agranat, C. Conti, *Nat. Photon.* **9**, 228 (2015).
- [7] H. Harutyunyan, *Nat. Photon.* **9**, 213 (2015).
- [8] R. Ilangoan, G. Ravi, C. Subramanian, P. Ramasamy, S. Sakai, *J. Crystal Growth* **237–239**, 694 (2002).
- [9] A.L. Gentile, F.H. Andres, *Mater. Res. Bull.* **2**, 853 (1967).
- [10] K.W. Goeking, R.K. Pandey, P.J. Squattrito, A. Clearfield, H.R. Beratan, *Ferroelectrics* **92**, 89 (1989).
- [11] M. Sasaura, T. Imai, H. Kohda, S. Tohno, M. Shimokozono, H. Fushimi, K. Fujiura, S. Toyoda, K. Enbutsu, A. Tate, K. Manabe, T. Matsuura, T. Kurihara, *J. Cryst. Growth* **275**, e2099 (2005).
- [12] S. Dagdale, V. Pahurkar, G. Muley, *Macromol. Symp.* **362**, 139 (2016).
- [13] J.Y. Wang, Q.C. Guan, J.Q. Wei, M. Wang, Y.G. Liu, *J. Cryst. Growth* **116**, 27 (1992).
- [14] K. Nakamura, J. Miyazu, M. Sasaura, K. Fujiura, *Appl. Phys. Lett.* **89**, 131115 (2006).
- [15] X. Yu, H. Wang, X. Rong, *Opt. Mater.* **46**, 429 (2015).
- [16] W. Ruan, G. Li, J. Zeng, L.S. Kamzina, H. Zeng, K. Zhao, L. Zheng, A. Ding, *J. Appl. Phys.* **110**, 074109 (2011).
- [17] K. Nakamura, J. Miyazu, Y. Sasaki, T. Imai, M. Sasaura, K. Fujiura, *J. Appl. Phys.* **104**, 013105 (2008).
- [18] J.E. Geusic, S.K. Kurtz, L.G. Van Uitert, S.H. Wemple, *Appl. Phys. Lett.* **4**, 141 (1964).
- [19] Q. Lu, J. Han, H. Dai, B. Ge, S. Zhao, *AIP Adv.* **5**, 087117 (2015).
- [20] S. Sang, Z. Yuan, L. Zheng, E. Sun, R. Zhang, J. Wang, R. Wang, B. Yang, M. Liu, *Opt. Mater.* **45**, 104 (2015).
- [21] G.-Z. Zhang, X.-R. Chen, H.-K. Yuan, A.-L. Kuang, H. Chen, *Phys. Status Solidi C* **14**, 1700026 (2017).
- [22] G.R.B.E. Romer, P. Bechtold, *Phys. Proced.* **56**, 29 (2014).